

Supplemental Figures

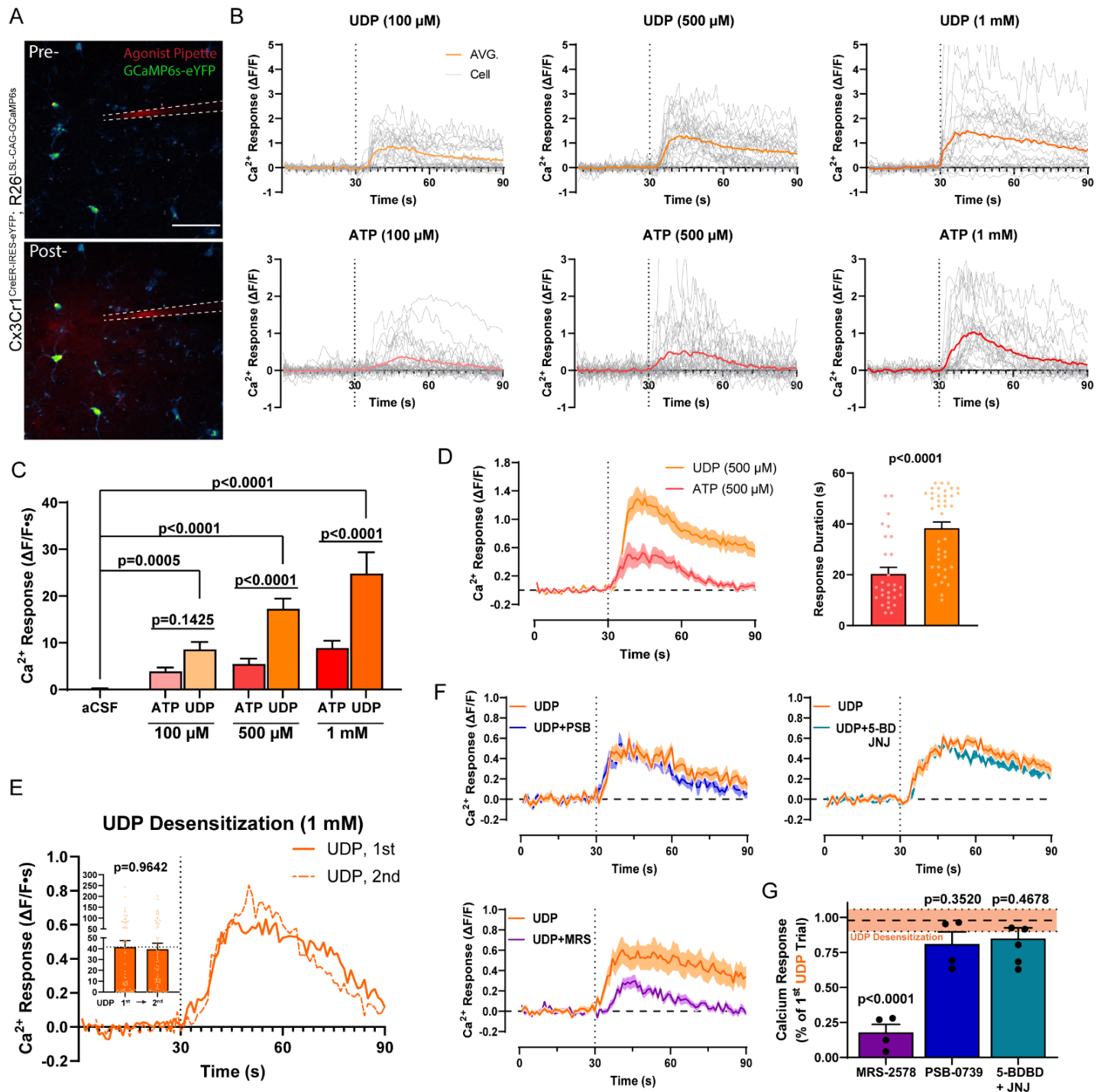


Figure S1: UDP signals through P2Y₆ receptors to evoke calcium signaling

(A) Image of an acute brain slice prepared from mice expressing GCaMP6s in microglia. An agonist is focally applied through a glass capillary with AlexaFluor 568 dye for visualization. Scale bar, 100 μ m. (B) Representative microglial calcium responses ($\Delta F/F$) to ATP or UDP application (dotted line represents time of agonist application). (C) Overall calcium responses in naive microglia to aCSF control or purine application. Two-Way ANOVA with Dunnett's post-hoc comparison between aCSF and UDP, or Sidak's post-hoc test for UDP vs ATP (4-6 slices prepared from N=3-4 mice;). (D) 500 μ M UDP or ATP calcium response duration (from paired trials in 3 slices from N=3 mice; dots represent ROIs; unpaired T-test). (E) Calcium responses to repeated UDP application to determine the effect of desensitization (line graph: average $\Delta F/F$ calcium responses to UDP from a representative paired trial; bar graph: overall UDP calcium response across paired trails in 4 slices from N=4 mice; dots represent ROIs; paired T-test). (F) Calcium responses to UDP alone and in a paired trial with bath-application of a selective antagonist (MRS-2578 (MRS, 40 μ M): P2Y₆ antagonist; PSB-0739 (PSB, 5 μ M): P2Y₁₂ antagonist; 5-BDBD (5-BD, 20 μ M): P2X₄ antagonist; JNJ-54175446 (JNJ, 10 μ M): P2X₇ antagonist). (G) Summary of antagonist effects on UDP calcium responses. One-Way ANOVA with Dunnett's post-hoc comparison to desensitization (orange horizontal line represents desensitization mean \pm SEM; dots represent an individual trial in one slice per mouse). All bar graphs or shaded line graphs represent the mean \pm SEM.

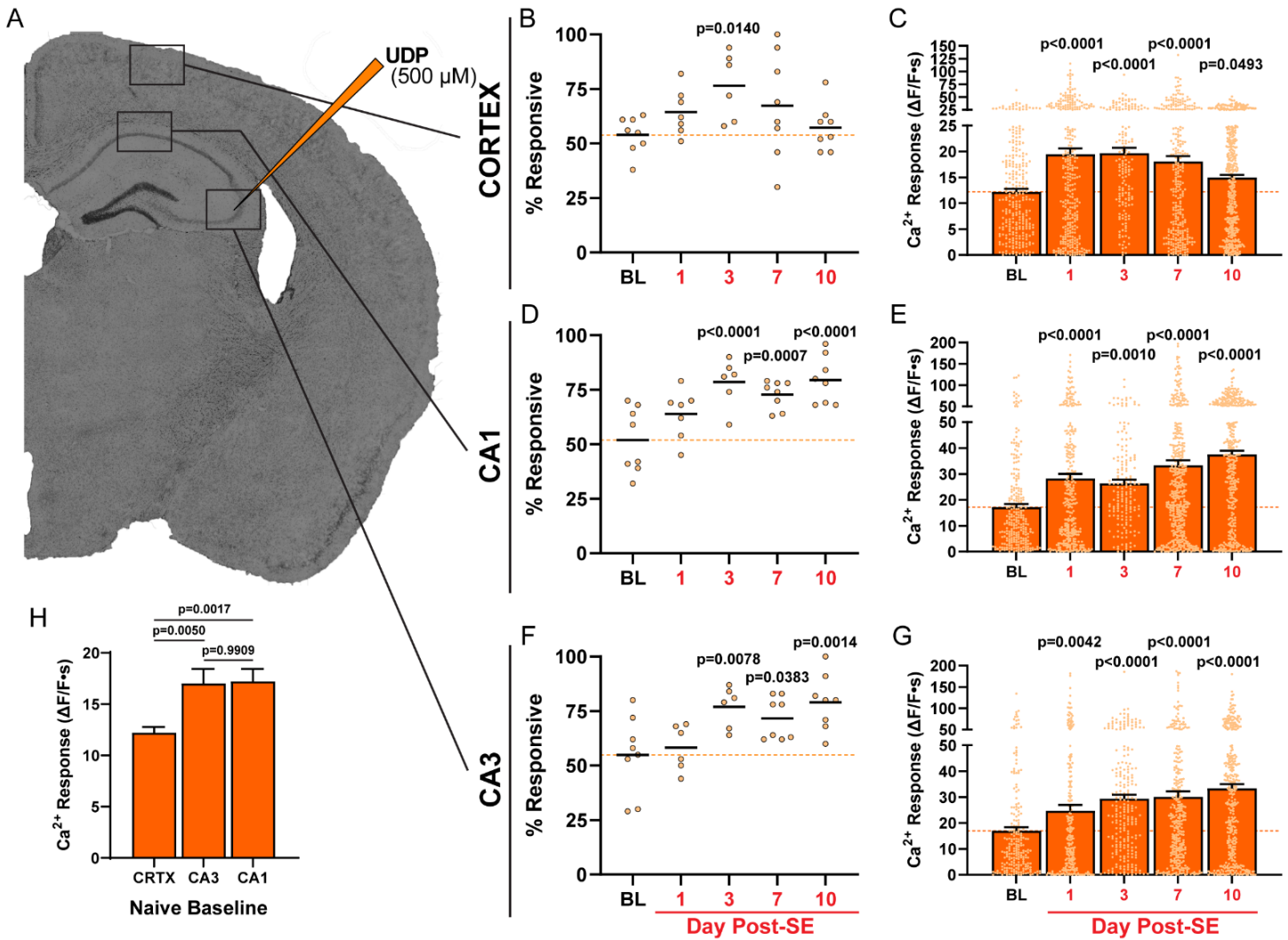


Figure S2: UDP calcium responses and spontaneous activity increase during early epileptogenesis in slice

(A) Regions surveyed in acute brain slice for microglial calcium responses. (B, D, F) The percentage of microglial ROIs responding to 500 μ M UDP application in cortex (B), CA1 (D), or CA3 (F). Dots represent an individual slice (2 per mouse, N=3-4). Line is at the mean. One-Way ANOVA with Dunnett's post-hoc comparison to baseline. (C, E, G) The calcium response from microglial ROIs after 500 μ M UDP application in cortex (C), CA1 (E), or CA3 (G). Dot represents an individual ROI (from 2 slices per mouse, N=3-4). One-Way ANOVA with Dunnett's post-hoc comparison to baseline. (H) Differences in baseline (naïve) microglial calcium responses to UDP between brain regions. One-Way ANOVA with Tukey's post-hoc comparison (data from all ROIs surveyed across 2 slices per mouse, N=4). Bars represent the mean \pm SEM.

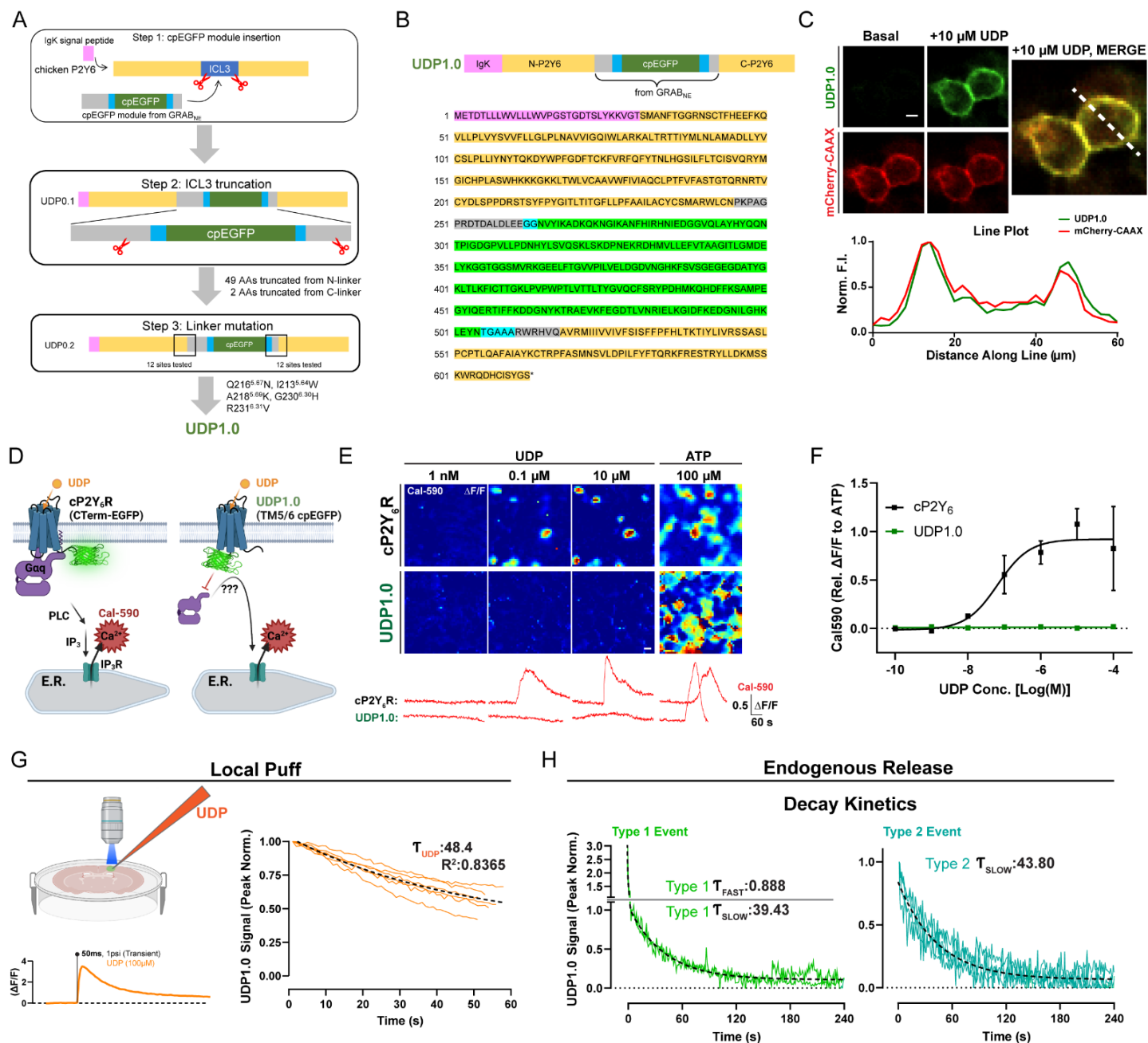


Figure S3: UDP sensor sequence, coupling, and kinetics, related to Figures 1 and 2

(A) Steps taken to optimize and refine UDP sensor signal. (B) Amino-acid sequence of UDP1.0. (C) Evaluation of UDP1.0 sensor trafficking to the membrane with membrane-trafficked mCherry-CAAX expression for reference. (D) Experimental schematic: Calbryte-590 calcium imaging in response to purines using HEK cells transfected with cP2Y₆ or UDP1.0. (E) Cal-590 calcium response images and corresponding $\Delta F/F$ traces from cP2Y₆- or UDP1.0-transfected HEK293T cells in response to purines. (F) ATP-normalized Cal-590 fluorescent responses across a range of UDP concentrations (mean \pm SEM; lines represent a non-linear fit of log (agonist) vs. 3-parameter response). (G) Schematic of *ex vivo*, local UDP application in a UDP1.0-transfected brain slice with a representative $\Delta F/F$ response. Peak-normalized responses were used to determine the UDP1.0 single-component T decay value in response to UDP (12 trials from 3 slices and mice). (H) One- or two-component T decay fits for Type 1 and Type 2 UDP events observed *in vivo* (T value reflects $n=15$ Type 1 and $n=22$ Type 2 events aggregated across $N=5$ mice).

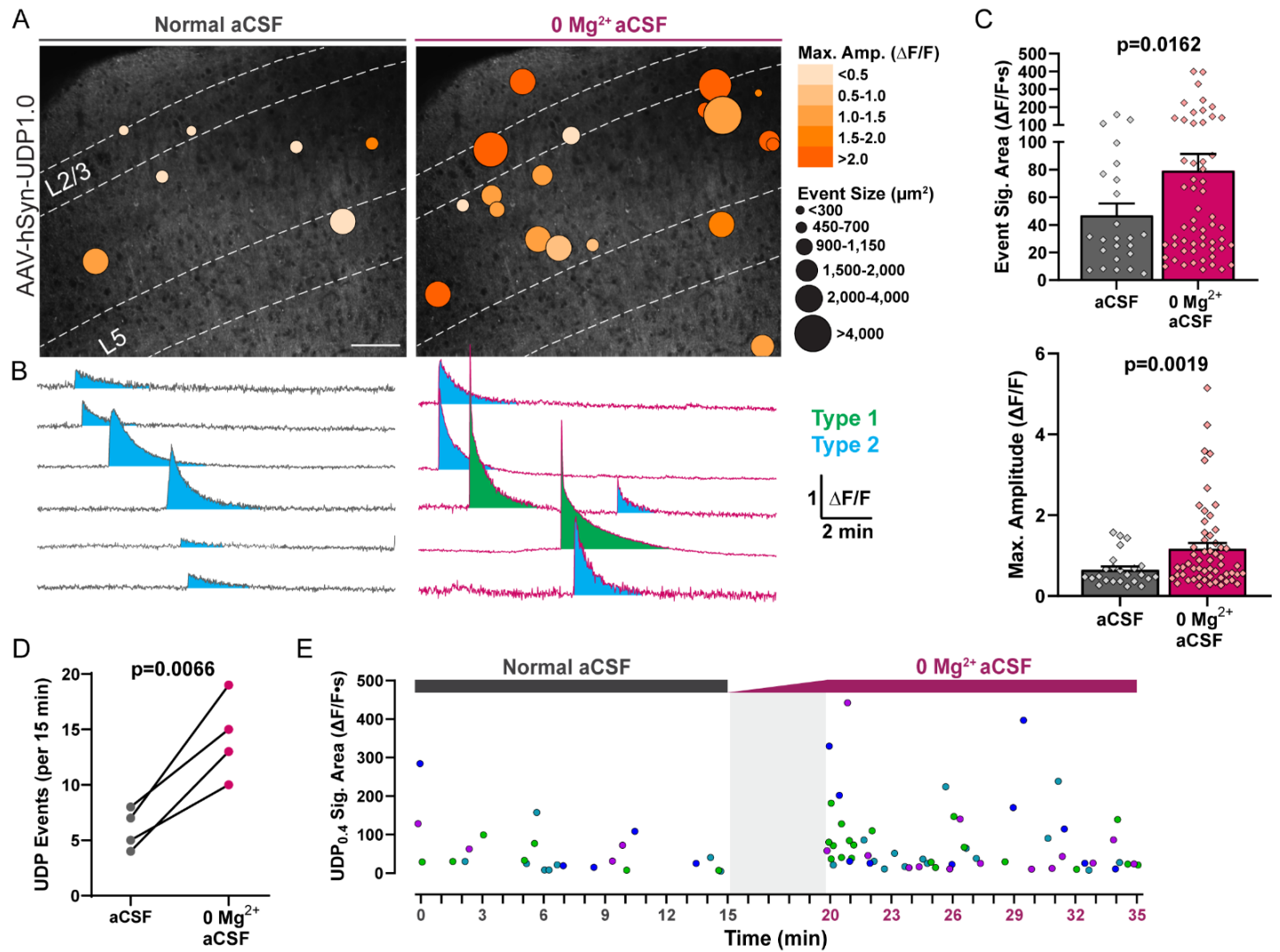


Figure S4: Enhanced UDP release during 0 Mg²⁺ hyperexcitability, related to Figure 2

(A) UDP1.0 sensor events overlaid across cortical layers during bath incubation with normal aCSF or 0 Mg²⁺ aCSF. Scale bar, 100 μm . (B) Event traces ($\Delta F/F$) demonstrating Type 2 events in the presence of normal aCSF, or a combination of Type 1 “sharp peak” events and Type 2 events during 0 Mg²⁺ conditions. (C) Comparison of UDP event signal area and maximum amplitude between normal and 0 Mg²⁺ aCSF conditions. Student’s t-test (dot: one event; bar: mean \pm SEM). (D) Paired UDP event frequency under normal and 0 Mg²⁺ aCSF conditions. Paired ratio T-test (one slice from N=4 mice). (E) Plot of UDP event signal area ($\Delta F/F \cdot s$) and timing over 15 min of normal aCSF incubation or 15 min of 0 Mg²⁺ aCSF incubation (gray box: 5 min solution exchange period; dot: one UDP event where color corresponds to a trial; one slice from N=4 mice).

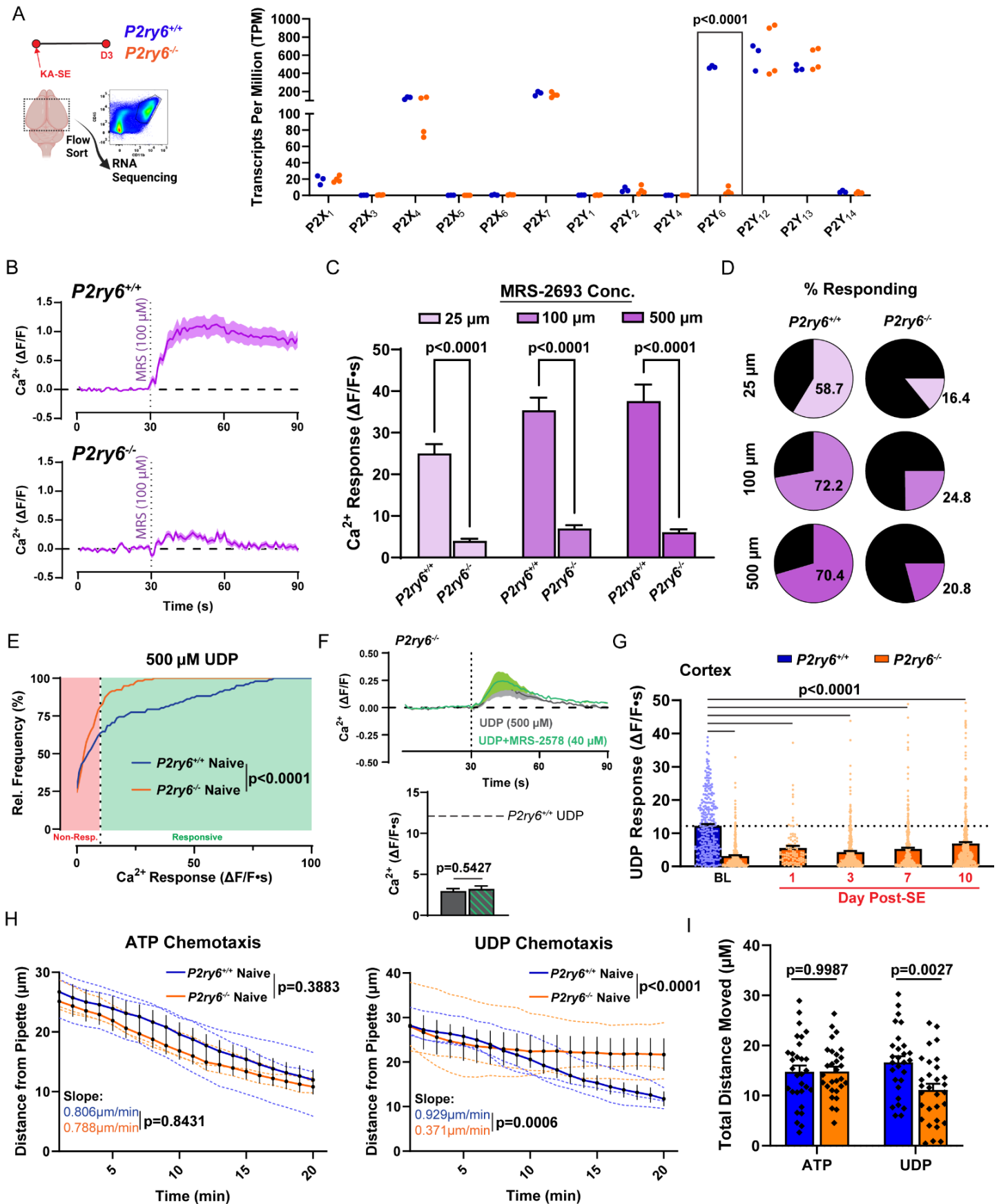


Figure S5: Functional characterization of the *P2ry6*^{-/-} mouse, related to Figure 3

(A) Isolation of microglia for transcriptomic analyses 3 days after KA-SE. Confirmation of *P2ry6* transcript loss from brain microglia without changes in other P2 receptors transcripts. Two-Way ANOVA with Sidak's post-hoc test (dot: one mouse/sample). (B) Representative *P2ry6*^{+/+} and *P2ry6*^{-/-} microglial calcium responses to MRS-2693, a high affinity P2Y₆ agonist, in naive brain slice. (C) Overall calcium

responses to MRS-2693 across a concentration range. Two-Way ANOVA with Sidak's post-hoc test (all concentrations tested in 2-3 trials per slice; 4 slices from N=4 mice per genotype). (D) Percentage of microglia responding to MRS-2693. (Average across trials; same dataset as C). (E) Distribution of microglial calcium responses to 500 μ M UDP by genotype. Welch's t-test of % responding ($\Delta F/F_s > 10$) by trial (2-3 trials per slice; 4 slices from N=4 mice per genotype). (F) Representative UDP calcium response in *P2ry6*^{-/-} slice in the absence or presence of bath MRS-2578, a P2Y₆-selective antagonist (top), and overall quantification (bottom; 4 slices from N=4 mice; unpaired t-test). (G) UDP calcium responses in brain slice at baseline and time points following KA-SE. One-Way ANOVA with Dunnett's post-hoc comparison to *P2ry6*^{-/-} baseline (2 slices/mouse from N=4 mice per group and time point; dot: individual ROI). (H) Microglial process chemotaxis towards a 1mM ATP- or UDP-containing glass pipette. Overall effect of genotype established by Two-Way ANOVA; Slope comparison established by simple linear regression (dotted lines: individual trial mean;). (I) Total distance moved by microglial processes over a 20 min trial. Two-Way ANOVA with Sidak's post-hoc test (dot: individual process; survey of 28-30 processes from 3 separate slices and animals per group). Bar graphs and shaded line graphs both display the mean \pm SEM.

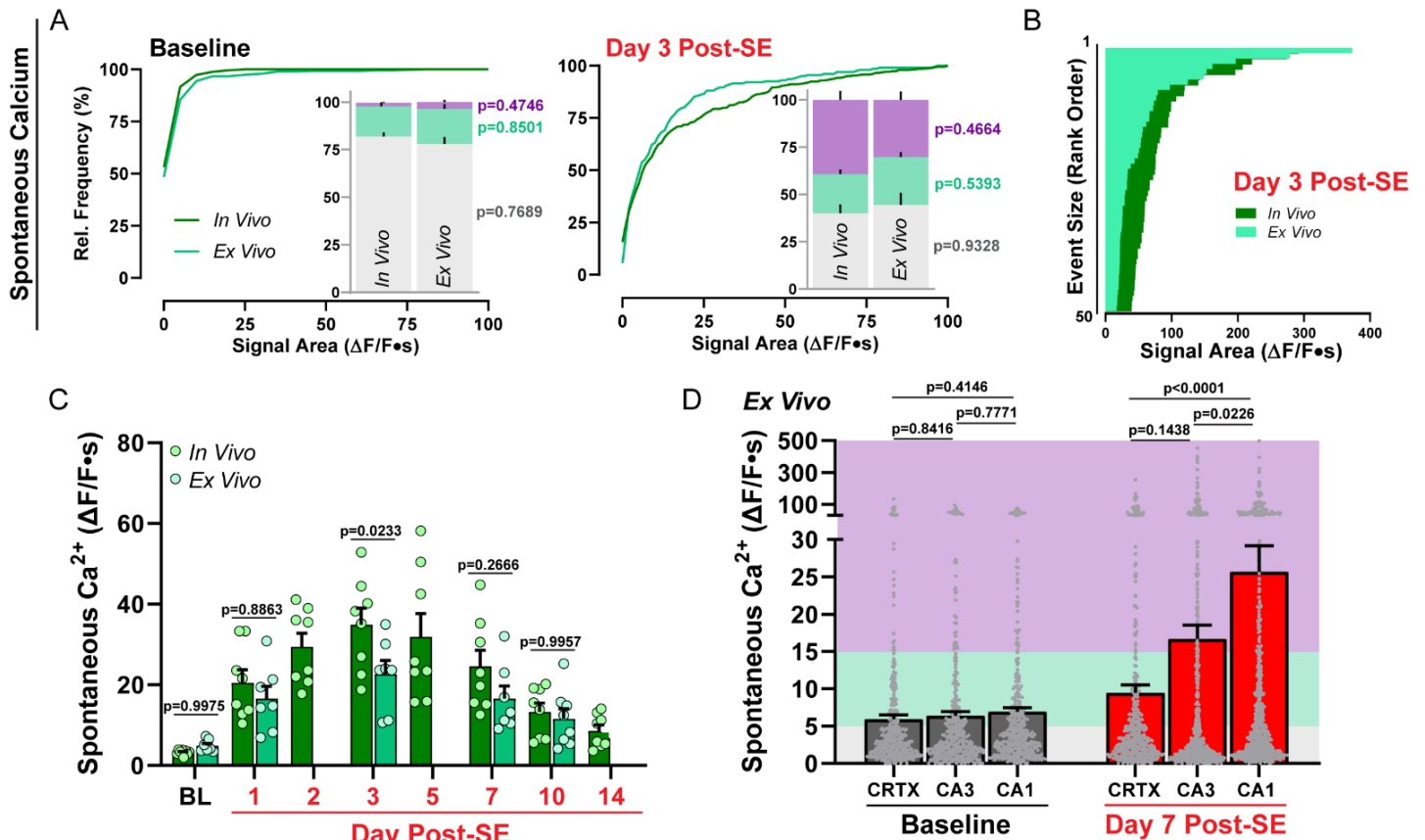


Figure S6: Comparison of spontaneous calcium activity between cortical microglia in slice and *in vivo*, related to Figure 3

(A) Cumulative distribution of spontaneous calcium activity recorded from cortical microglia *in vivo* (chronic cranial window) and *ex vivo* (acute coronal brain slice) at baseline and 3 days after KA-SE. Bar graphs compare the percentage of microglial ROIs which are inactive (gray bar, $\Delta F/F < 5$), display low activity (teal bar, $5 < \Delta F/F \leq 15$), or are highly active (purple bar, $\Delta F/F > 15$). Two-way ANOVA with Sidak's post-hoc comparison between activity levels. (B) Rank order of the largest calcium events *in vivo* and *ex vivo* in cortex on day 3 after KA-SE. (C) Microglial spontaneous calcium signaling in cortex for *in vivo* and *ex vivo* preparations. Two-way ANOVA with Sidak's post-hoc test (dot: average spontaneous calcium activity across all ROIs from a chronic window field of view (*in vivo*) or *ex vivo* slice field of view; both are 300 x 300 μ m). (D) Comparison of WT microglial spontaneous calcium activity in brain slice by region and time point. One-way ANOVA with Tukey's post-hoc test by time point (dots represent individual ROIs). Bars represent the mean \pm SEM. *In vivo* data come from N=4 WT mice with two regions surveyed longitudinally; *ex vivo* data come from N=4 WT mice per time point with up to two brain slices surveyed per mouse.

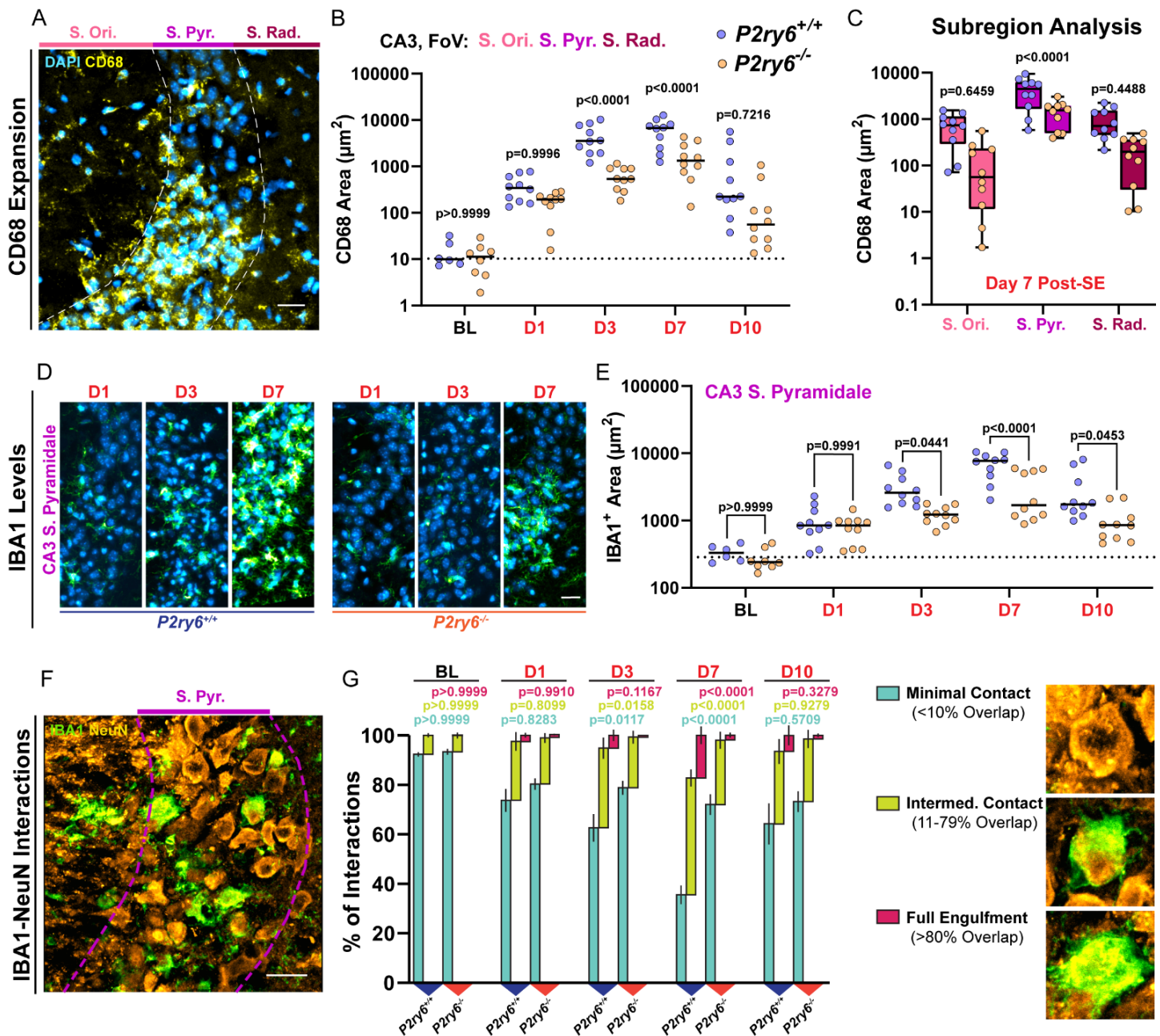


Figure S7: Evolution of phagocytic interactions in CA3, related to Figure 4

(A) Image of CD68 staining in CA3 from a day 7 post-SE WT mouse. Scale bar, 20 μm . (B) Quantification of CD68 area over time from the entire CA3 field of view. Two-Way ANOVA with Sidak's post-hoc test. (C) CD68 staining between genotypes day 7 post-SE by CA3 subregion. One-Way ANOVA with Sidak's post-hoc test. (D) Representative images of IBA1 (green) in the CA3 pyramidal band during early epileptogenesis. Scale bar, 20 μm . (E) Quantification of IBA1 area over time in the CA3 pyramidal band. Two-Way ANOVA with Sidak's post-hoc test. (F) IBA1 and NeuN cell interactions layer day 7 post-SE in the CA3 pyramidal layer of a WT mouse. Scale bar, 20 μm . (G) Percentage of CA3 NeuN neurons having minimal/no contact with IBA1 cells, intermediate contact, or reaching full engulfment criteria across time (examples on the right). Two-Way ANOVA with Sidak's post-hoc test by interaction type. Bars represent the mean \pm SEM. Dots represent one of two hippocampi surveyed per mouse. N=3-5 mice per group.

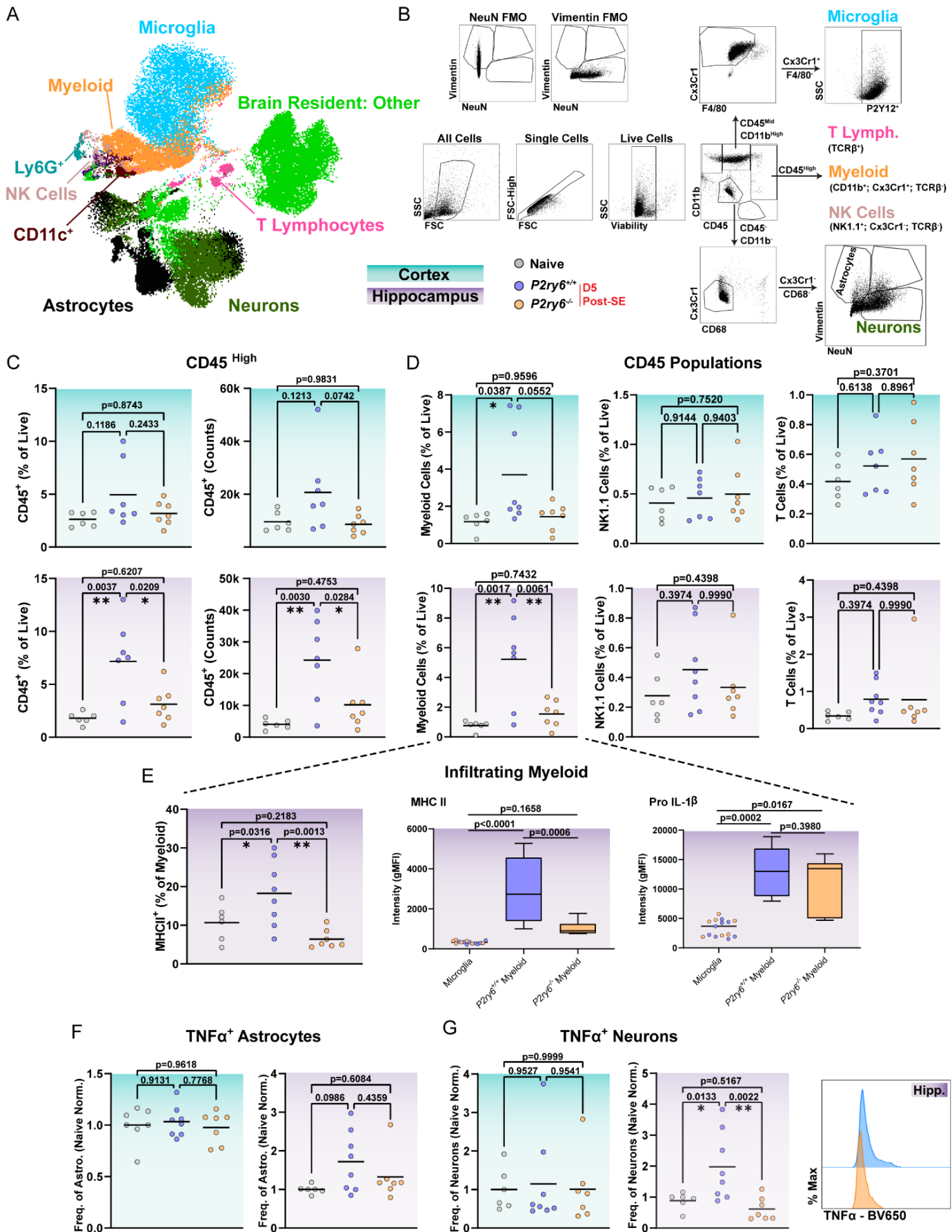


Figure S8: Greater pro-inflammatory myeloid infiltration occurs in *P2ry6*^{+/+} hippocampus, related to Figure 6

(A) UMAP of resident and infiltrating cell populations built off FSC, SSC, all surface markers and cytokines (see STAR Methods). (B) Gating strategy to separate microglia, infiltrating immune populations, and other resident brain cells. (C) The number (counts) and

frequency (% live) of CD45⁺ immune cell populations between regions and genotypes. (D) Further evaluation of infiltrating CD45^{High} cells based upon markers defining myeloid, NK, or T lymphocyte sub-populations. (E) Differences in MHCII expression frequency and intensity (gMFI) between infiltrating myeloid population in *P2ry6*^{+/+} and *P2ry6*^{-/-} hippocampus and in reference to resident microglia. Pro IL-1 β expression in infiltrating myeloid cells relative to resident microglia. (F) Evaluation of TNF α expression frequency and intensity by vimentin⁺ astrocytes in cortex and hippocampus. (G) Expression of TNF α in NeuN⁺ neurons, including frequency, gMFI intensity, and mode-normalized representative histograms. Data come from N=6 naïve mice (4 WT, 2 KO), N=8 *P2ry6*^{+/+} mice and N=7 *P2ry6*^{-/-} mice from two independent cohorts. Scatter plots: dot represents one mouse, line at the mean. Box and whisker plots display mean, interquartile range, and min to max. Significance testing utilized a One-Way ANOVA with Tukey's post-hoc test.

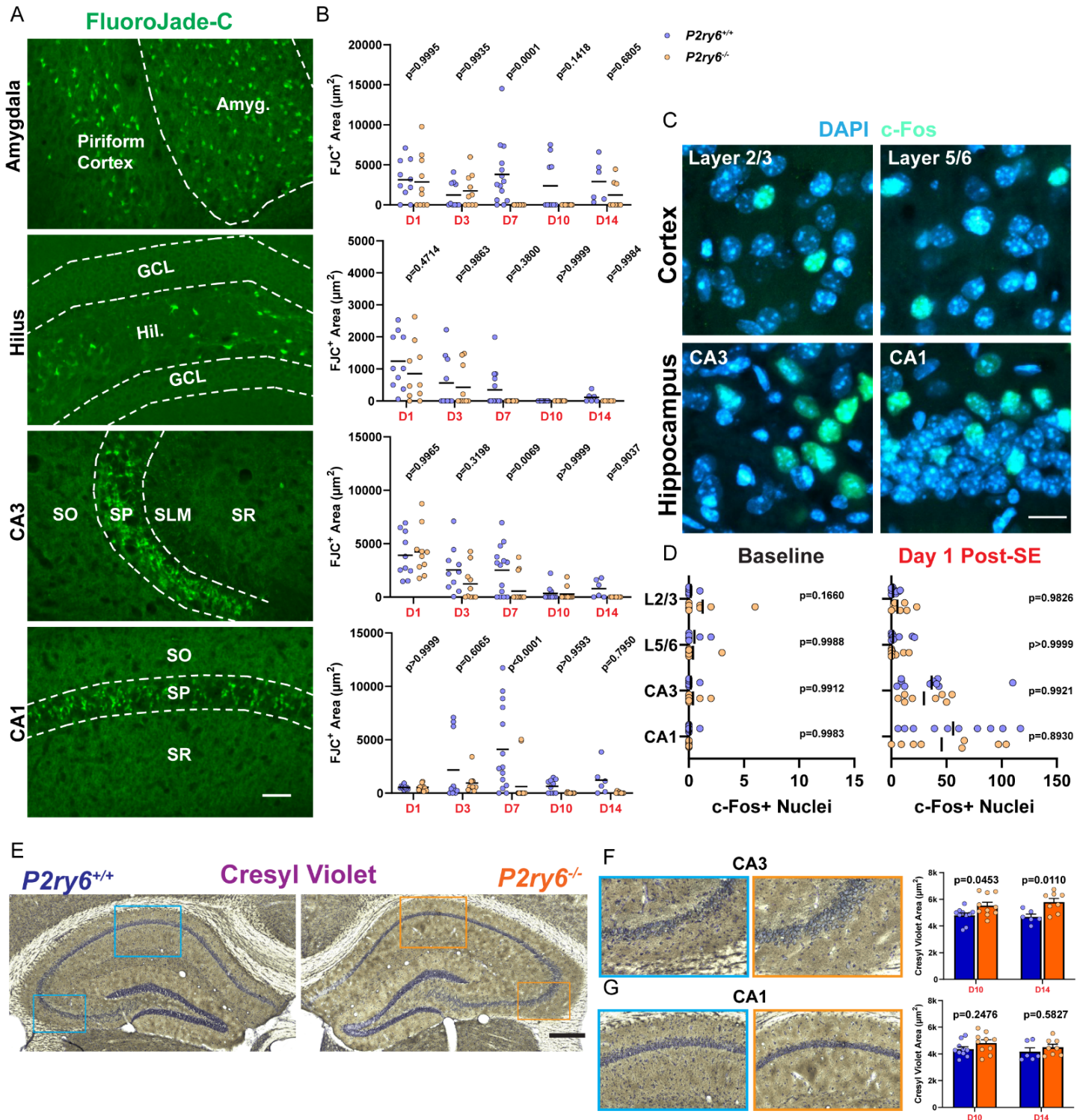


Figure S9: Comparison of neuropathology and seizure damage between genotypes, related to Figure 7

(A) Representative images of FluoroJade-C (FJC) staining one day after KA-SE in the amygdala, hilus, CA3, and CA1 regions. Scale bar, 50 μm . (GCL-Granule Cell Layer). (B) Quantification of FJC-positive cell area by region. Two-Way ANOVA with Sidak's post-hoc comparison (dot: one region; bilateral survey from N=3-9 mice per group). (C) Examples of DAPI and c-Fos staining one day after KA-SE. Scale bar, 15 μm . (D) Quantification of c-Fos positive nuclei between genotypes at baseline and one-day after KA-SE. Two-Way ANOVA with Sidak's post-hoc test by region (dot: one region; bilateral survey from N=4-5 mice per group). (E) Representative hippocampi stained with Cresyl Violet acetate 14 days after KA-SE. Scale bar, 500 μm . (F,G) Enlarged images of the CA3 (F) and CA1 (G) regions with corresponding quantification of Cresyl Violet area within the pyramidal band. Two-Way ANOVA with Sidak's post-hoc test (dot: one region; bilateral survey from N=3-5 mice per group).